An idealized $1\frac{1}{2}$-layer isentropic model with convection and precipitation for satellite data assimilation research. Part II: model derivation

Onno Bokhove[*1], Luca Cantarello[†1], and Steven Tobias[1]

[1]School of mathematics, University of Leeds, Leeds, UK

Abstract

In this part II paper we present the analytical derivation of the isentropic $1\frac{1}{2}$-layer shallow water model described and used in part I of this study. The mathematical derivation presented here is based on a combined asymptotic and slaved Hamiltonian analysis. The scaling assumptions throughout the paper are supported by real observations based on radiosonde data. Eventually, a fully consistent isentropic $1\frac{1}{2}$-layer model emerges from imposing fluid at rest ($\mathbf{v}_1 = 0$) and zero Montgomery potential ($M_1 = 0$) in the upper layer of an isentropic two-layer model.

1 Introduction

In Part I, we presented and discussed both the dynamics and the numerics of a new idealised model (*ismodRSW*) to be used in future satellite data assimilation experiments. In this paper, or Part II, we show the formal mathematical derivation of the underlying isentropic $1\frac{1}{2}$-layer shallow water model.

Shallow water models represent a class of simplified fluid-dynamic models often utilized to describe analytically and numerically a number of fundamental and theoretical properties of stratified fluids, including the effect of rotation (e.g. as in the Rossby adjustment problem) and the propagation of gravity waves. In recent decades, shallow water models have also been utilised as idealised tools in data assimilation research, for both oceanic and atmospheric applications (Žagar et al., 2004; Salman et al., 2006; Stewart et al., 2013; Würsch and Craig, 2014; Kent et al., 2017).

Mathematically, shallow water models emerge after vertically integrating the Navier-Stokes equations whenever the vertical motions can be neglected over wider zonal and meridional scales. The derivation of a simplified, isopycnal single-layer shallow water model (i.e. a model with a single layer of fluid at constant density) is typical textbook material and can be found in many places (see, for example, §2 in the introduction of Zeitlin (2007)). The derivation of multi-layer shallow water models is also covered extensively in many books (see, for instance, chapter 3 of Vallis (2017)). $1\frac{1}{2}$-layer models represent further simplifications in which the fluid is capped by a rigid lid and hence the total fluid depth is conserved in time. An isopycnal $1\frac{1}{2}$-layer model differs from a single-layer model only in the definition of the gravity acceleration g and a *reduced* gravity g' is introduced:

$$g' = \frac{\rho_2 - \rho_1}{\rho_2} g, \tag{1}$$

in which ρ_1 and ρ_2 indicate the densities of the fluid in the upper and lower layer, with the least dense layer on top, i.e., $\rho_2 > \rho_1$. Moving from an isopycnal model (constant density) to an isentropic one (constant potential temperature) requires the derivation of a different set of equations, obtained here with the help of Hamiltonian mechanics (exploiting a slaved Hamiltonian approach) and the introduction of fast and slow variables (cf., Van Kampen (1985)) arising from an asymptotic analysis performed on an isentropic two-layer shallow water model.

The need for a Hamiltonian derivation arises from the fact that simply imposing a rigid-lid approximation on an isentropic two-layer model leads to an apparent inconsistency in the model derivation, in which a zero Montgomery potential constraint

---

*Corresponding author: o.bokhove@leeds.ac.uk
†Corresponding author: mmlca@leeds.ac.uk

in the top layer ($M_1 = 0$) seems not to be preserved in time by the continuity equations.

In this regard, the derivation of balanced fluid dynamical models exploiting Hamilton's principle in which high-frequency waves are filtered out started with the work of Salmon (1983, 1985, 1988). In particular, the use of Dirac brackets' theory (Dirac, 1958, 1964) applied to the Hamiltonian derivation of multi-layer shallow water models was developed further in Bokhove (2002a) and Vanneste and Bokhove (2002). The derivation of an N–layer isentropic shallow water model based on Hamiltonian mechanics was given in Bokhove and Oliver (2009) and will constitute the starting point of our study. In this regard, the reader might find useful to know that parts of the work treated in this paper has appeared in a previously unpublished manuscript (Bokhove, 2007).

The structure of the paper is as follows. In section 2, we start with presenting the equations of a full two-layer isentropic model and show how imposing a rigid lid condition leads to a seemingly inconsistent yet closed $1\frac{1}{2}$-layer model. In section 3 we introduce a scaling for the two-layer model and its equations are subsequently non-dimensionalized; afterward, an asymptotic analysis based on the method of multiple timescales is conducted. In section 4 we use radiosonde observations to justify the scaling used in the asymptotic analysis. In section 5, the Hamiltonian derivation of the isentropic $1\frac{1}{2}$-layer shallow water model is discussed. Conclusions are given in section 6.

2 A rigid-lid approximation in a two-layer model

We start this section by presenting an isentropic two-layer model and finish with an argument how a closed $1\frac{1}{2}$-layer model emerges by taking a seemingly inconsistent rigid-lid approximation. That the final model is nonetheless consistent will be subsequently shown in a combined asymptotic and Hamiltonian analysis, resulting in a rigid-lid condition with a (nearly) passive and high upper layer. The Hamiltonian derivation demonstrates that the $1\frac{1}{2}$-layer model has a bonafide conservative and hyperbolic structure, which is exploited in the numerical discretization discussed in Part I.

A full, geometric derivation of an isentropic N–layer model can be found in Bokhove and Oliver (2009). Here, we take a two-layer simplification thereof, with $N = 2$. Figs. 1a,c provide a sketch of the two-layer model configuration. The momentum equations of the model arise by assuming hydrostatic balance and constant entropy (potential temperature θ) in each layer. The continuity equations emerge once the space (x, y) and time-dependent (t) pseudo-density $\sigma_\alpha(x, y, t)$ for each layer, numbered by $\alpha = 1, 2$, is defined, i.e.:

$$\sigma_\alpha = p_r \left(\eta_\alpha - \eta_{\alpha-1} \right) / g, \tag{2}$$

in which g refers to the gravity acceleration and $\eta_\alpha - \eta_{\alpha-1}$ is the net non-dimensional pressure difference between the bottom and the top of the layer α, with η defined as $\eta = p/p_r$ for a reference pressure p_r. The pseudo-density σ arises from hydrostatic balance $\mathrm{d}p = -\rho g \, \mathrm{d}z$, integrating an element of mass flux for some infinitesimal surface element $\mathrm{d}A$: $\mathrm{d}m/\mathrm{d}A = \rho \, \mathrm{d}z = -\mathrm{d}p/g$ across each layer with density ρ, pressure p, and the gravitational acceleration g. In Bokhove (2002b) and Ripa (1993) the variational and Hamiltonian formulation of the isentropic N–layer equations are derived by simplifying the Eulerian variational principle of the compressible Euler equations.

The resulting four, isentropic two-layer (continuity and momentum) equations are the following:

$$\partial_t \sigma_\alpha + \nabla \cdot (\sigma_\alpha \mathbf{v}_\alpha) = 0, \tag{3a}$$

$$\partial_t \mathbf{v}_\alpha + (\mathbf{v}_\alpha \cdot \nabla)\mathbf{v}_\alpha + f \mathbf{v}_\alpha^\perp = -\nabla M_\alpha, \tag{3b}$$

with $\alpha = 1, 2$ and in which: ∇ is the horizontal gradient, $\mathbf{v}_\alpha = \mathbf{v}_\alpha(x, y, t) = (u_\alpha, v_\alpha)^T$ is the horizontal velocity within layer α and $\mathbf{v}_\alpha^\perp = (-v_\alpha, u_\alpha)^T$ the vector perpendicular to it, f is the Coriolis frequency, and M_α is the Montgomery potential. In order to close the system, one needs to specify the Montgomery potentials in each layer. As seen in section §3 of Bokhove and Oliver (2009), for a two-layer model these potentials can be defined as:

$$M_1 = c_p \, \theta_2 \, \eta_2{}^\kappa + c_p (\theta_1 - \theta_2) \eta_1^\kappa + g z_2, \tag{3c}$$

$$M_2 = c_p \, \theta_2 \, \eta_2{}^\kappa + g z_2, \tag{3d}$$

in which $\kappa = R/c_p$ is the ratio between the specific gas constant for dry air ($R = 287 \, \mathrm{JKg}^{-1}\mathrm{K}^{-1}$) and its specific heat capacity at constant pressure ($c_p = 1004 \, \mathrm{JKg}^{-1}\mathrm{K}^{-1}$).

The hydrostatic condition for an isentropic model $\partial M/\partial z = 0$ implies that, in general, the Montgomery potential $M = c_p \theta \eta^\kappa + g z$ is independent of z within each layer. Therefore, one can evaluate M in the bottom layer (where $\theta = \theta_2$) at both $z = z_2$ and $z = z_1$, and M in the upper layer (where $\theta = \theta_1$) at both $z = z_1$ and $z = z_0$, to find:

$$g z_0 = c_p \, \theta_1 \left(\eta_1^\kappa - \eta_0^\kappa \right) + g z_1, \tag{4a}$$

$$g z_1 = c_p \, \theta_2 \left(\eta_2^\kappa - \eta_1^\kappa \right) + g z_2, \tag{4b}$$

from which is possible to express the thickness of each layer as:

$$h_1 = z_0 - z_1 = (c_p \, \theta_1/g) \, (\eta_1^\kappa - \eta_0^\kappa), \tag{5a}$$

$$h_2 = z_1 - z_2 = (c_p \, \theta_2/g) \, (\eta_2^\kappa - \eta_1^\kappa). \tag{5b}$$

We note here that the non-dimensional pressure η_0 is treated as a constant throughout the paper.
Finally, the relations between layer pressure and pseudo-densities can be derived using the expressions (2) for σ_1 and σ_2 as follows:

$$\eta_1 = g \, \sigma_1/p_r + \eta_0 \qquad \text{and} \qquad \eta_2 = g \, (\sigma_1 + \sigma_2)/p_r + \eta_0. \tag{6}$$

When one takes a rigid-lid approximation, it is convenient to add a constant $K = -(c_p \theta_1 \eta_0^\kappa + g Z_0)$ to M_1 in (3c), leading to:

$$M_1 = c_p \, \theta_1 \, (\eta_1^\kappa - \eta_0^\kappa) + c_p \, \theta_2 \, (\eta_2^\kappa - \eta_1^\kappa) + g z_2 - g Z_0. \tag{7}$$

Therefore, by substituting (4b) into (4a) and subtracting $g Z_0$ from both sides one finds:

$$g z_0 = c_p \, \theta_1 \, (\eta_1^\kappa - \eta_0^\kappa) + c_p \, \theta_2 \, (\eta_2^\kappa - \eta_1^\kappa) + g z_2,$$
$$g z_0 - g Z_0 = c_p \, \theta_1 \, (\eta_1^\kappa - \eta_0^\kappa) + c_p \, \theta_2 \, (\eta_2^\kappa - \eta_1^\kappa) + g z_2 - g Z_0,$$
$$g z_0 - g Z_0 = M_1.$$

If the top surface is fixed, i.e. $z_0 = Z_0$, then $M_1 = g \, (z_0 - Z_0) = 0$, and a closed $1\frac{1}{2}$-layer model emerges as follows (a sketch of the model is given in Figs.1b,d). For the $1\frac{1}{2}$-layer model, the momentum equations in the lower stratospheric layer remain as in equations (3a,b) for $\alpha = 2$. The model is indeed closed, because $M_1 = 0$ defines $\eta_1 = p_1/p_r$ in terms of $\eta_2 = p_2/p_r$. This fact allows σ_2 to be expressed in terms of η_2 as follows: $\sigma_2(\eta_2) = p_r \, (\eta_2 - \eta_1(\eta_2))/g$. We note that such a $1\frac{1}{2}$-layer model has the advantage over a one-layer model that the pressure p_1 is active and not constrained to be constant, as is p_0. Consequently, the values of the surface pressure p_2 are more realistic. At first sight, the $1\frac{1}{2}$-layer model, however, seems inconsistent, since the constraint $M_1 = 0$ is not preserved in time by the original two continuity equations. Nevertheless – as we will show later in this paper – the closed $1\frac{1}{2}$-layer model (3a,b) with $\alpha = 2$ and Montgomery potential M_2 results after taking $M_1 = 0$ and $\mathbf{v}_1 = 0$ in the momentum equation of the stratospheric layer. Perhaps not surprisingly, the original potential energy of the two-layer model subject to the constraint $M_1 = g \, (z_0 - Z_0) = 0$ does give the desired potential energy of the $1\frac{1}{2}$-layer model.

3 Scaling of a two-layer model and asymptotic analysis

3.1 Non-dimensionalization and scaling of the two-layer model

In order to perform asymptotic analysis on the two-layer model, we first non-dimensionalize the equations (3) by applying the following scaling:

$$(x, y) = L \, (x^*, y^*), \quad t = (L/U_2) \, t^*, \quad \mathbf{v}_\alpha = U_\alpha \mathbf{v}_\alpha^*, \quad M_\alpha = g \, H_\alpha \, M_\alpha^*,$$
$$\nabla = (1/L) \nabla^*, \quad \sigma_1 = (p_r/g) \, \sigma_1^* = (p_r/g) \, (\Sigma_1 + \varepsilon^2 \, \sigma_1'), \quad \sigma_2 = \varepsilon^2 \, (p_r/g) \, \sigma_2^*,$$
$$p_\alpha = p_r \eta_\alpha, \quad \theta_\alpha = (g \, H_1/c_p) \, \theta_\alpha^*, \quad h_\alpha = H_\alpha \, h_\alpha^*,$$
$$Z_0 = H_1 \, Z_0^*, \quad z_2 = \text{Fr}_2^2 \, H_2 \, z_2^*, \tag{8}$$

together with the following scaling approximations:

$$\sqrt{\text{Fr}_1} \approx \varepsilon, \quad \text{and} \quad \delta_a \text{Fr}_2^2 \approx \varepsilon^2;$$

in which: L is the horizontal length scale; U_α and H_α are the layer velocity and depth scale respectively; Σ_1 is a constant; Fr_α indicates the layer Froude number $\text{Fr}_\alpha = U_\alpha/\sqrt{g H_\alpha}$; $c_p \theta_1/g H_1$ is assumed to be of order $O(1)$; ε is the layer velocity ratio $\varepsilon = U_1/U_2$; $\delta_a = H_2/H_1$ defines the layer thickness ratio. Both ε and δ_a are assumed to be small. We will discuss in section §4 to what extent the chosen scaling is supported by observations.
After dropping the asterisks, the scaling (8) substituted in (5) yields:

$$h_1 = \frac{c_p}{g H_1} \frac{g H_1}{c_p} \theta_1 \left(\eta_1^\kappa - \eta_0^\kappa \right) = \theta_1 \left(\eta_1^\kappa - \eta_0^\kappa \right) = \theta_1 \left(\sigma_1^\kappa - \eta_0^\kappa \right), \tag{9a}$$

$$h_2 = \frac{c_p}{g H_2} \frac{g H_1}{c_p} \theta_2 \left(\eta_2^\kappa - \eta_1^\kappa \right) = \frac{\theta_2}{\delta_a} \left(\eta_2^\kappa - \eta_1^\kappa \right) = \frac{\theta_2}{\delta_a} \left(\left(\sigma_1 + \varepsilon^2 \sigma_2 \right)^\kappa - \sigma_1^\kappa \right), \tag{9b}$$

in which we use (6), and make the assumption that η_0 is small compared to (non-dimensional) σ_1. Again, the validity of the latter on observational evidence is discussed in section §4; nevertheless, even in absence of such hypothesis, the rest of the derivation would only differ for the presence of an additional constant.

By substituting (8) further into (3), dropping the asterisks on the scaled variables and after some reordering, we obtain the following system of equations:

$$\partial_t \sigma_1' + \varepsilon \nabla \cdot (\sigma_1' \mathbf{v}_1) + \frac{1}{\varepsilon} \nabla \cdot (\Sigma_1 \mathbf{v}_1) = 0, \tag{10a}$$

$$\partial_t \mathbf{v}_1 + \varepsilon \left(\mathbf{v}_1 \cdot \nabla \mathbf{v}_1 + \frac{1}{\text{Ro}_1} \mathbf{v}_1^\perp \right) + \frac{1}{\varepsilon} \nabla M_1' = 0, \tag{10b}$$

$$\partial_t \sigma_2 + \nabla \cdot (\sigma_2 \mathbf{v}_2) = 0, \tag{10c}$$

$$\partial_t \mathbf{v}_2 + \mathbf{v}_2 \cdot \nabla \mathbf{v}_2 + \frac{1}{\text{Ro}_2} \mathbf{v}_2^\perp + \nabla M_2' = 0, \tag{10d}$$

with Ro_α being the layer Rossby number $\text{Ro}_\alpha = U_\alpha / (fL)$ and potentials M_1' and M_2' defined as:

$$M_1' = \theta_1 \left((\Sigma_1 + \varepsilon^2 \sigma_1')^\kappa - (\Sigma_1)^\kappa \right) / \varepsilon^2 +$$
$$\theta_2 \left((\Sigma_1 + \varepsilon^2 \sigma_1' + \varepsilon^2 \sigma_2)^\kappa - (\Sigma_1 + \varepsilon^2 \sigma_1')^\kappa \right) / \varepsilon^2 + z_2, \tag{11}$$
$$M_2' = \theta_2 \left((\Sigma_1 + \varepsilon^2 \sigma_1' + \varepsilon^2 \sigma_2)^\kappa - (\Sigma_1)^\kappa \right) / \varepsilon^2 + z_2.$$

In deriving equation (11), the following mean potentials $\bar{M}_1$ and $\bar{M}_2$ have been introduced (a full derivation can be found in Appendix A):

$$\bar{M}_1 = \theta_1 (\Sigma_1)^\kappa - \theta_1 \eta_0^\kappa - Z_0 \quad \text{and} \quad \bar{M}_2 = \frac{\theta_2}{\delta_a} (\Sigma_1)^\kappa.$$

As will appear clearer in both the asymptotic analysis and the Hamiltonian derivation, these mean potentials are chosen primarily to avoid singularities at leading order in ε.

3.2 Asymptotic analysis: method of multiple timescales

Asymptotic analysis of the upper layer at leading order in ε – that is at $\mathcal{O}(1/\varepsilon)$ in (10) – yields two constraints:

$$\phi_1 = M_1'|_{\varepsilon=0} = 0 \qquad \text{and} \qquad D_1 = \nabla \cdot (\Sigma_1 \mathbf{v}_1) = 0, \tag{12}$$

with leading order potentials (obtained by computing the Taylor expansions of (11) around $\sigma_1' = 0$, $\sigma_2 = 0$):

$$M_1'|_{\varepsilon=0} = \kappa \Sigma_1^{\kappa-1} (\theta_1 \sigma_1' + \theta_2 \sigma_2) + z_2 \quad \text{and}$$
$$M_2'|_{\varepsilon=0} = \kappa \theta_2 (\Sigma_1)^{\kappa-1} (\sigma_1' + \sigma_2) + z_2. \tag{13}$$

We introduce a fast time scale $\tau = t/\varepsilon$ and evaluate (10) at leading order; that is, we truncate the system (10) and (11) at the fast time scale by taking the limit $\varepsilon \to 0$ (after multiplication by ε). The following linear wave equations then appear after some manipulation:

$$\partial_\tau \sigma_1' + D_1 = 0, \qquad \partial_\tau D_1 = -\nabla \cdot (\Sigma_1 \nabla M_1'|_{\varepsilon=0}),$$
$$\partial_\tau \omega_1 = 0, \qquad \partial_\tau \sigma_2 = 0, \qquad \partial_\tau \mathbf{v}_2 = 0, \tag{14}$$

with vorticity $\omega_1 = \nabla^\perp \cdot \mathbf{v}_1$. The system (14) shows that the fast variables σ_1' and D_1 oscillate rapidly, while the slow variables ω_1, σ_2 and $\mathbf{v}_2$ vary on the slow time scale. The introduction of fast and slow variables is based on the distinction between high-frequency and low-frequency waves in linearized wave equations (Van Kampen, 1985). Later in section §5, we will consider the reduced, Hamiltonian dynamics on the "slow" manifold defined by the constraints (12).

4 Observations supporting the scaling

The validity of the scaling used in section 3 determines whether the $1\frac{1}{2}$-layer model to be derived in this paper is suitable to represent the real atmosphere. In this sense, here we show two possible applications: one in the stratosphere and one in the troposphere, with the latter being more relevant for the purpose of part I of this study, as convection and precipitation are confined therein. Table 1 summarizes the values derived from real atmospheric measurements (i.e. from radiosonde data) of the main relevant physical quantities together with the associated non-dimensional parameters Fr_1^{obs}, Fr_2^{obs}, δ_a and ε. A sketch of the model configuration for both cases is shown in Fig. 1.

4.1 Two-layer stratosphere

The scaling is compatible with a $1\frac{1}{2}$-layer approximation of the stratosphere. In this regard, our estimates are based on zonally averaged climatological seasonal radiosonde data displayed in Birner (2006), where potential temperature and horizontal wind speed are displayed as function of height and latitude. On request, Dr. Birner extracted vertical profiles of potential temperature and pressure at about 57.25^oN (i.e. at mid-latitudes) versus height in the summer season, shown in Fig. 2. From the data, it seems reasonable to take $Z_2 = 10.6$km for the tropopause height (the lower bound) and, say, $Z_1 = 16.6$km and $Z_0 = 34.6$km. Hence, $H_2^{\text{obs}} = 6$km and $H_1^{\text{obs}} = 18$km. Estimates for the horizontal velocities are $U_1^{\text{obs}} \approx 2$m/s and $U_2^{\text{obs}} \approx 14$m/s (from Fig. 7 of Birner (2006); and personal communication). From Fig. 2, average values of the potential temperature are found to be approximately $\theta_2^{\text{obs}} = 381$K and $\theta_1^{\text{obs}} = 672$K. Likewise, pressures observed and deduced at these heights are $p_2^{\text{obs}} = 242$ mb, $p_1^{\text{obs}} = 97$ mb, and $p_0^{\text{obs}} = 6.2$ mb, and therefore $\eta_0 \ll \sigma_1$. In our scaling, $\text{Fr}_1^{\text{obs}}, \text{Fr}_2^{\text{obs}}, \varepsilon, \delta_a, \theta_1$ and p_1 follow, for example, after choosing $\theta_2^{\text{obs}}, H_1^{\text{obs}}, H_2^{\text{obs}}, p_2^{\text{obs}}, p_0^{\text{obs}}, U_1^{\text{obs}}, U_2^{\text{obs}}$ and exploiting eqs. (5). Further constants used are $g = 9.81\,\text{m}\,\text{s}^{-1}$, $c_p = 1004.6\,\text{J}\,\text{kg}^{-1}\,\text{K}^{-1}$, $R = 287.04\,\text{J}\,\text{kg}^{-1}\,\text{K}^{-1}$ and $p_r = 1000\,\text{mb}$ such that $\kappa = 2/7$. We obtain $\text{Fr}_1^{\text{obs}} \approx 0.0048, \text{Fr}_2^{\text{obs}} \approx 0.0577, \varepsilon \approx 0.14, \delta_a \approx 0.33, \theta_1 = 629$K (solving (5a) for theta1) and $p_1 = 97$mb (solving (5b) for η_1 and hence p_1). All data are reported in Table 1. This pressure value compares well with the observed one, while the calculated and observed potential temperature differ somewhat because the observed buoyancy frequency (and temperature) is roughly constant and not the entropy as in our layer model. The values of the Froude numbers Fr_1 and Fr_2 deduced from the scaling parameters ε and δ_a are within a factor 5 from those deduced from the observations Fr_1^{obs} and Fr_2^{obs}. For the above values, $c_p \theta_1/(g H_1) = 3.58$. Despite these slight differences, the data provide an observational basis for the chosen scaling.

4.2 Two-layer troposphere in presence of a low-level Jet

The scaling presented in section 3 is also compatible with a $1\frac{1}{2}$-layer approximation in the troposphere. Low-level jets (LLJs) are recurrent meteorological features located at various locations in the world (Rife et al., 2010) and they happen to be particularly common over the Great Plains in the Southern United States (Ladwig, 1980; Djurić and Damiani Jr, 1980).

Fig. 3 shows vertical profiles obtained from radiosonde data of both potential temperature and wind speed during a LLJ event on 10th–11th December 1977 in Brownsville, Texas (US). We use this as a case study to provide a justification for the scaling chosen in section 3. We approximate the troposphere as a two-layer fluid, exploiting the discontinuities in the potential temperature profile of Fig. 3(b) as a reference. Mean potential temperature values of $\theta_1^{\text{obs}} = 311.0$ K and $\theta_2^{\text{obs}} = 291.8$ K follow after taking $H_1^{\text{obs}} = 4.02$ km and $H_2^{\text{obs}} = 2.08$ km in Fig. 3(b). The above values of θ_1^{obs} and θ_2^{obs} are used as a constraint to compute H_1^{obs} and H_2^{obs} also in the profiles of Figs. 3(a)-(c), in virtue of the isentropic assumption (i.e. constant potential temperature within each layer). Once layer depths in each profile are established, mean wind speed values U_1^{obs} and U_2^{obs} within each layer are also computed (dashed line in Fig. 3). Table 1 summarizes all the other relevant physical parameters associated with the radiosonde data plotted in Fig. 3, including the values of pressure $p_0^{\text{obs}}, p_1^{\text{obs}}$ and p_2^{obs} obtained for each profile (vertical profiles of pressure not shown). In this case, $\eta_0 > \sigma_1$. All in all, it is possible to see from Table 1 how ε and δ_a lie below one during the LLJ event; moreover, the rigid lid condition leading to the $1\frac{1}{2}$-layer configuration appears to be justified, as the variation in height of $Z_0 = H_1 + H_2 = \{6\,\text{km}, 6.1\,\text{km}, 6.25\,\text{km}\}$ is smaller than the change in depth of the bottom layer $H_2 = \{2.02\,\text{km}, 2.08\,\text{km}, 1.65\,\text{km}\}$. Furthermore, the values of p_1 and θ_1 computed via eq. (5) using the observed values $\theta_2^{\text{obs}}, H_1^{\text{obs}}, H_2^{\text{obs}}, p_2^{\text{obs}}, p_0^{\text{obs}}$ are very close to p_1^{obs} and θ_1^{obs} coming from the observations themselves. The values of the Froude numbers Fr_1 and Fr_2 deduced from the scaling parameters ε and δ_a are on average (cf. rightmost column in Table 1) within a factor 8 from those deduced from the observations Fr_1^{obs} and Fr_2^{obs}. Finally, $c_p \theta_1^{\text{obs}}/(g H_1^{\text{obs}}) \approx \{8.00, 7.92, 6.92\}$ for the three vertical profiles of Fig.3 . Overall, the data support the scaling (8) chosen in section 3.

5 Hamiltonian derivation

5.1 Constrained Hamiltonian formulation of the $1\frac{1}{2}$-layer equations

A dimensional Hamiltonian formulation of the two-layer system is introduced to derive the formulation for the $1\frac{1}{2}$-layer system. It consists of the evolution:

$$\frac{\text{d}\mathcal{F}}{\text{d}t} = \{\mathcal{F}, \mathcal{H}\}, \tag{15}$$

with the shallow-layer generalized Poisson bracket in both layers ($\alpha = 1, 2$):

$$\{\mathcal{F}, \mathcal{G}\} = \sum_{\alpha=1}^{2} \iint \left[q_\alpha \left(\frac{\delta\mathcal{F}}{\delta\mathbf{v}_\alpha}\right)^\perp \cdot \frac{\delta\mathcal{G}}{\delta\mathbf{v}_\alpha} - \frac{\delta\mathcal{F}}{\delta\sigma_\alpha} \boldsymbol{\nabla} \cdot \frac{\delta\mathcal{G}}{\delta\mathbf{v}_\alpha} + \frac{\delta\mathcal{G}}{\delta\sigma_\alpha} \boldsymbol{\nabla} \cdot \frac{\delta\mathcal{F}}{\delta\mathbf{v}_\alpha} \right] \text{d}x\text{d}y, \tag{16}$$

for arbitrary functionals $\mathcal{F}$ and $\mathcal{G}$ of $\{\mathbf{v}_\alpha, \sigma_\alpha\}$ and a Hamiltonian of the type:

$$\mathcal{H} = \iint \left[\sum_{\alpha=1}^{2} \left(\frac{1}{2} \sigma_\alpha |\mathbf{v}_\alpha|^2 + g\,\sigma_\alpha\,z_2 \right) + \frac{p_r\,c_p\,\theta_2}{g\,(\kappa+1)} \left(\eta_2^{\kappa+1} - \eta_1^{\kappa+1} \right) \right.$$
$$\left. + \frac{p_r\,c_p\,\theta_1}{g\,(\kappa+1)} \eta_1^{\kappa+1} - \sigma_1 \left(c_p\,\theta_1\,\eta_0^\kappa + g\,Z_0 \right) \right] \mathrm{d}x\mathrm{d}y, \tag{17}$$

and the potential vorticity q_α in each layer α:

$$q_\alpha = (f + \nabla^\perp \cdot \mathbf{v}_\alpha)/\sigma_\alpha, \tag{18}$$

appearing in (16). The bracket (16) is the same as that in Bokhove (2002b). The Hamiltonian follows either directly from the Eulerian or parcel Eulerian-Lagrangian momentum equations or from the Hamiltonian of the 3D Euler equations by neglecting the vertical velocity relative to the horizontal velocities, by using hydrostatic balance and the ideal gas law, and integration in the vertical over each isentropic layer. In the latter integration, the horizontal velocity is assumed to be independent of the depth in each layer and the last term in (17) is then absent, whereupon the resulting Hamiltonian matches (3.16) in Bokhove (2002b) after noting that the layer numbers are the same but the levels are numbered starting from 1 at the top. This last term, linear in σ_1, arises without problem because any multiple of the mass $\iint \sigma_1 \, \mathrm{d}x\mathrm{d}y$ in the upper layer is a Casimir invariant and can be added to the Hamiltonian without changing the dynamics (cf. Shepherd (1990)). After taking the variation, it amounts to adding a constant to the Montgomery potential, which is always allowed. This addition further ensures that $M_1 = g\,(z_0 - Z_0)$, which is a useful simplification as we have seen.

The functional derivatives of the Hamiltonian (17) are:

$$\frac{\delta\mathcal{H}}{\delta\mathbf{v}_\alpha} = \sigma_\alpha\,\mathbf{v}_\alpha \qquad \text{and} \qquad \frac{\delta\mathcal{H}}{\delta\sigma_\alpha} = |\mathbf{v}_\alpha|^2/2 + M_\alpha, \tag{19}$$

with which it can be verified that (15) yields the equations of motion (3) in both layers when we choose the functionals:

$$\mathcal{F} = \mathbf{v}_\alpha(\mathbf{x}, t) = \iint \delta(\mathbf{x} - \mathbf{x}')\,\mathbf{v}_\alpha(\mathbf{x}', t)\,\mathrm{d}x'\mathrm{d}y' \quad \text{and}$$

$$\mathcal{F} = \sigma_\alpha(\mathbf{x}, t) = \iint \delta(\mathbf{x} - \mathbf{x}')\,\sigma_\alpha(\mathbf{x}', t)\,\mathrm{d}x'\mathrm{d}y',$$

respectively (see, e.g., Shepherd (1990); Salmon (1988), for an introduction on Hamiltonian fluid dynamics), in which the first expression can be separated into two scalar quantities defined for each velocity component $\mathbf{v}_\alpha = (u_\alpha, v_\alpha)$. The second part of (19) follows from (17) after some calculation using the definitions of the Montgomery potentials in (3c) and (3d) and the pseudo-density (6) in (3).

The formulation (15)–(17) is Hamiltonian as the bracket $\{\mathcal{F}, \mathcal{G}\}$ is antisymmetric (i.e. $\{\mathcal{F}, \mathcal{G}\} = -\{\mathcal{G}, \mathcal{F}\}$) and satisfies the Jacobi identity, i.e.:

$$\{\mathcal{F}, \{\mathcal{G}, \mathcal{K}\}\} + \{\mathcal{G}, \{\mathcal{K}, \mathcal{F}\}\} + \{\mathcal{K}, \{\mathcal{F}, \mathcal{G}\}\} = 0 \tag{20}$$

for arbitrary functional $\mathcal{F}, \mathcal{G}$ and $\mathcal{K}$.

In the verification of the properties above (as well as in some others later in the paper), certain integral terms vanish in presence of certain boundary conditions such as: periodic boundaries; quiescence and constancy at infinity where σ_α is constant and $\mathbf{v}_\alpha = 0$; slip flow along walls, such that $\mathbf{v}_\alpha \cdot \hat{\mathbf{n}} = 0$ with $\hat{\mathbf{n}}$ the outward-pointing normal to the wall; or a combinations of these. Henceforth in this section, we use for simplicity periodic boundary conditions or quiescence and constancy at infinity. Furthermore, in these verifications the functional derivatives have to be restricted to satisfy corresponding boundary conditions. Once that the Hamiltonian formulation for the two-layer model is established, we can use (8) to scale the Hamiltonian dynamics as follows:

$$\frac{\mathrm{d}\mathcal{F}}{\mathrm{d}t} = \{\mathcal{F}, \mathcal{H}\}$$
$$= \iint \left[\varepsilon\,q_1 \left(\frac{\delta\mathcal{F}}{\delta\mathbf{v}_1} \right)^\perp \cdot \frac{\delta\mathcal{H}}{\delta\mathbf{v}_1} - \frac{1}{\varepsilon} \frac{\delta\mathcal{F}}{\delta\sigma_1'} \nabla \cdot \frac{\delta\mathcal{H}}{\delta\mathbf{v}_1} + \frac{1}{\varepsilon} \frac{\delta\mathcal{H}}{\delta\sigma_1'} \nabla \cdot \frac{\delta\mathcal{F}}{\delta\mathbf{v}_1} + \right.$$
$$\left. q_2 \left(\frac{\delta\mathcal{F}}{\delta\mathbf{v}_2} \right)^\perp \cdot \frac{\delta\mathcal{H}}{\delta\mathbf{v}_2} - \frac{\delta\mathcal{F}}{\delta\sigma_2} \nabla \cdot \frac{\delta\mathcal{H}}{\delta\mathbf{v}_2} + \frac{\delta\mathcal{H}}{\delta\sigma_2} \nabla \cdot \frac{\delta\mathcal{F}}{\delta\mathbf{v}_2} \right] \mathrm{d}x\mathrm{d}y \tag{21}$$

in which we have scaled the Hamiltonian with $p_r\,U_1^2\,L^2/g$ and the functional derivatives with $1/L^2$, with potential vorticities:

$$q_1 = (1/\mathrm{Ro}_1 + \omega_1)/(\Sigma_1 + \varepsilon^2\,\sigma_1') \qquad \text{and} \qquad q_2 = (1/\mathrm{Ro}_2 + \nabla^\perp \cdot \mathbf{v}_2)/\sigma_2, \tag{22}$$

and modified Hamiltonian:

$$
\begin{aligned}
\mathcal{H} = \iint \Bigg[& \frac{1}{2}\left(\Sigma_1 + \varepsilon^2\,\sigma_1'\right)|\mathbf{v}_1|^2 + \sigma_1'\,z_2 + \frac{1}{2}\,\sigma_2\,|\mathbf{v}_2|^2 + \sigma_2\,z_2 \\
& + \frac{1}{\varepsilon^4}\,\frac{\theta_2}{\kappa+1}\left(\left(\Sigma_1 + \varepsilon^2\,\sigma_1' + \varepsilon^2\,\sigma_2\right)^{\kappa+1} - \left(\Sigma_1 + \varepsilon^2\,\sigma_1'\right)^{\kappa+1}\right) + \\
& - \frac{1}{\varepsilon^4}\,\theta_1\,(\Sigma_1)^{\kappa+1} + \frac{\theta_1}{\varepsilon^4}\,\frac{1}{\kappa+1}\left(\Sigma_1 + \varepsilon^2\,\sigma_1'\right)^{\kappa+1} \\
& - \frac{\left(\theta_1\,\sigma_1' + \theta_2\,\sigma_2\right)}{\varepsilon^2}\,(\Sigma_1)^{\kappa} \Bigg]\,\mathrm{d}x\mathrm{d}y.
\end{aligned}
\tag{23}
$$

The additional terms, constant and linear in σ_1' and σ_2, are added to obtain a Hamiltonian of $\mathcal{O}(1)$ that is non-singular as $\varepsilon \to 0$. These extra terms arise because mass is globally conserved in each layer and can be introduced formally by adding constants and mass Casimirs $C_1 = \lambda_1 \iint (\Sigma_1 + \varepsilon^2\,\sigma_1')\,\mathrm{d}x\,\mathrm{d}y$ and $C_2 = \lambda_2 \iint \varepsilon^2\,\sigma_2\,\mathrm{d}x\,\mathrm{d}y$ to the original, scaled Hamiltonian $\tilde{\mathcal{H}}$ for suitable choices of λ_1 and λ_2 (more details are given in in Appendix B). These above Casimirs are conserved since $\mathrm{d}C_1/\mathrm{d}t = \{C_1, \tilde{\mathcal{H}}\} = 0$ and $\mathrm{d}C_2/\mathrm{d}t = \{C_2, \tilde{\mathcal{H}}\} = 0$. The above expression is related but not quite equivalent to the available potential energy (Shepherd, 1993). Here it suffices to note that it yields the proper equations of motion. Akin to the dimensional case, the variational derivatives of (23) are readily calculated to be:

$$
\frac{\delta\mathcal{H}}{\delta\sigma_1'} = \varepsilon^2\,|\mathbf{v}_1|^2/2 + M_1', \quad \frac{\delta\mathcal{H}}{\delta\sigma_2} = |\mathbf{v}_2|^2/2 + M_2',
$$

$$
\frac{\delta\mathcal{H}}{\delta\mathbf{v}_1} = \left(\Sigma_1 + \varepsilon^2\,\sigma_1'\right)\mathbf{v}_1 \quad \text{and} \quad \frac{\delta\mathcal{H}}{\delta\mathbf{v}_2} = \sigma_2\,\mathbf{v}_2.
\tag{24}
$$

Finally, the substitution of (24) into (21) yields the scaled equations of motion (10) with (11).

Given the constraints $\phi_1' = M_1' = 0$ and $D_1 = \nabla \cdot (\Sigma_1 \mathbf{v}_1) = 0$, we can transform the generalized Poisson bracket (21) in terms of the six variables $(\mathbf{v}_\alpha, \sigma_1', \sigma_2)$ to the variables $(\phi_1', D_1, \omega_1, \mathbf{v}_2, \sigma_2)$ with $\omega_1 = \nabla^\perp \cdot \mathbf{v}_1$ being the vorticity in the top layer. The functional derivatives with respect to the former variables relate to those in terms of the latter variables as follows (see Appendix C):

$$
\left.\frac{\delta\mathcal{F}}{\delta\mathbf{v}_1}\right|_{\sigma_1'} = -\left(\nabla^\perp\frac{\delta\mathcal{F}}{\delta\omega_1} + \Sigma_1\,\nabla\frac{\delta\mathcal{F}}{\delta D_1}\right), \quad \left.\frac{\delta\mathcal{F}}{\delta\mathbf{v}_2}\right|_{\sigma_1'} = \left.\frac{\delta\mathcal{F}}{\delta\mathbf{v}_2}\right|_{\phi_1}
$$

$$
\left.\frac{\delta\mathcal{F}}{\delta\sigma_1'}\right|_{\mathbf{v}_1} = \frac{\partial M_1'}{\partial\sigma_1'}\frac{\delta\mathcal{F}}{\delta\phi_1}, \quad \left.\frac{\delta\mathcal{F}}{\delta\sigma_2}\right|_{\mathbf{v}_1,\sigma_1'} = \left.\frac{\delta\mathcal{F}}{\delta\sigma_2}\right|_{\phi_1} + \frac{\partial M_1'}{\partial\sigma_2}\frac{\delta\mathcal{F}}{\delta\phi_1},
\tag{25}
$$

in which the subscripts on the left-hand sides are used to avoid confusion on which set of variables is considered. After substitution of (25) into (21) and some rearrangement, we find:

$$
\begin{aligned}
\frac{\mathrm{d}\mathcal{F}}{\mathrm{d}t} = \{\mathcal{F},\mathcal{H}\} = \iint \Bigg[& \varepsilon\,q_1\,J\left(\frac{\delta\mathcal{F}}{\delta\omega_1},\frac{\delta\mathcal{H}}{\delta\omega_1}\right) + \varepsilon\,(\Sigma_1)^2\,q_1\,J\left(\frac{\delta\mathcal{F}}{\delta D_1},\frac{\delta\mathcal{H}}{\delta D_1}\right) + \\
& \varepsilon\,\Sigma_1\,q_1\left[\left(\nabla\frac{\delta\mathcal{H}}{\delta\omega_1}\right)\cdot\nabla\frac{\delta\mathcal{F}}{\delta D_1} - \left(\nabla\frac{\delta\mathcal{F}}{\delta\omega_1}\right)\cdot\nabla\frac{\delta\mathcal{H}}{\delta D_1}\right] + \\
& \frac{1}{\varepsilon}\frac{\partial M_1'}{\partial\sigma_1'}\left[\frac{\delta\mathcal{F}}{\delta\phi_1}\nabla\cdot\left(\Sigma_1\nabla\frac{\delta\mathcal{H}}{\delta D_1}\right) - \frac{\delta\mathcal{H}}{\delta\phi_1}\nabla\cdot\left(\Sigma_1\nabla\frac{\delta\mathcal{F}}{\delta D_1}\right)\right] + \\
& q_2\frac{\delta\mathcal{F}}{\delta\mathbf{v}_2}^\perp\cdot\frac{\delta\mathcal{H}}{\delta\mathbf{v}_2} - \left(\frac{\delta\mathcal{F}}{\delta\sigma_2} + \frac{\partial M_1'}{\partial\sigma_2}\frac{\delta\mathcal{F}}{\delta\phi_1}\right)\nabla\cdot\frac{\delta\mathcal{H}}{\delta\mathbf{v}_2} + \\
& \left(\frac{\delta\mathcal{H}}{\delta\sigma_2} + \frac{\partial M_1'}{\partial\sigma_2}\frac{\delta\mathcal{H}}{\delta\phi_1'}\right)\nabla\cdot\frac{\delta\mathcal{F}}{\delta\mathbf{v}_2} \Bigg]\,\mathrm{d}x\,\mathrm{d}y
\end{aligned}
\tag{26}
$$

with $J(a,b) := (\partial_x a)(\partial_y b) - (\partial_x b)(\partial_y a)$ being the Jacobian operator. Note that, from (22), it follows that q_α is $\mathcal{O}(1)$. From (26) we derive the following system of equations for the new set of variables $(\phi_1', D_1, \omega_1, \mathbf{v}_2, \sigma_2)$:

$$
\begin{aligned}
\frac{\partial \phi_1(x,y,t)}{\partial t} &= \{\phi_1(x,y,t), \mathcal{H}\} \\
&= \frac{1}{\varepsilon} \frac{\partial M_1'}{\partial \sigma_1'} \nabla \cdot \left(\Sigma_1 \nabla \frac{\delta \mathcal{H}}{\delta D_1} \right) - \frac{\partial M_1'}{\partial \sigma_2} \nabla \cdot \frac{\delta \mathcal{H}}{\delta \mathbf{v}_2}, \\
\frac{\partial D_1(x,y,t)}{\partial t} &= \{D_1(x,y,t), \mathcal{H}\} \\
&= -\varepsilon \nabla \cdot \left(\Sigma_1 q_1 \nabla \frac{\delta \mathcal{H}}{\delta \omega_1} \right) + \varepsilon J\left(\frac{\delta \mathcal{H}}{\delta D_1}, \Sigma_1^2 q_1 \right) - \frac{1}{\varepsilon} \nabla \cdot \left(\Sigma_1 \nabla \left(\frac{\partial M_1'}{\partial \sigma_1'} \frac{\delta \mathcal{H}}{\delta \phi_1} \right) \right), \\
\frac{\partial \omega_1(x,y,t)}{\partial t} &= -\varepsilon J(q_1, \frac{\delta \mathcal{H}}{\delta \omega_1}) + \varepsilon \nabla \cdot \left(\Sigma_1 q_1 \nabla \frac{\delta \mathcal{H}}{\delta D_1} \right), \\
\frac{\partial \mathbf{v}_2(x,y,t)}{\partial t} &= -q_2 \nabla^\perp \frac{\delta \mathcal{H}}{\delta \mathbf{v}_2} - \nabla \left(\frac{\delta \mathcal{H}}{\delta \sigma_2} + \frac{\partial M_1'}{\partial \sigma_2} \frac{\delta \mathcal{H}}{\delta \phi_1} \right), \\
\frac{\partial \sigma_2(x,y,t)}{\partial t} &= -\nabla \cdot \frac{\delta \mathcal{H}}{\delta \mathbf{v}_2}.
\end{aligned}
\tag{27}
$$

At leading order in ε the variational derivative of the Hamiltonian (23) is (see Appendix D):

$$
\delta \mathcal{H}|_{\varepsilon=0} = \iint \left[-\chi \, \delta D_1 - \Psi \, \delta \omega_1 + M_1'|_{\varepsilon=0} \, \delta \sigma_1' + \sigma_2 \, \mathbf{v}_2 \cdot \delta \mathbf{v}_2 + \right.
$$
$$
\left. \left(\frac{1}{2} |\mathbf{v}_2|^2 + M_2'|_{\varepsilon=0} \right) \delta \sigma_2 \right] dx\,dy,
\tag{28}
$$

in which we have used $\Sigma_1 \mathbf{v}_1 = \Sigma_1 \nabla \chi + \nabla^\perp \Psi$ with velocity potential χ and (transport) streamfunction Ψ. Therefore, using (28) one finds:

$$
\left. \frac{\delta \mathcal{H}}{\delta D_1} \right|_{\varepsilon=0} = -\chi \qquad \text{and} \qquad \left. \frac{\delta \mathcal{H}}{\delta \sigma_1'} \right|_{\varepsilon=0} = M_1'|_{\varepsilon=0}.
\tag{29}
$$

By evaluating (27) at leading order in ε one obtains:

$$
\varepsilon \frac{\partial \phi_1}{\partial t} \propto D_1 = 0 \qquad \text{and} \qquad \varepsilon \frac{\partial D_1}{\partial t} \propto \nabla \cdot (\Sigma_1 \nabla M_1'|_{\varepsilon=0}) = 0,
\tag{30}
$$

producing the constraints (12) as a solution, which shows consistency at leading order. Hence, at leading order in ε we take $\delta \mathcal{H}/\delta \phi_1|_{\varepsilon=0} = \delta \mathcal{H}/\delta D_1|_{\varepsilon=0} = 0$ and from (27) we find the balanced dynamics on the slow manifold; that is, we truncate the dynamics to the leading order terms in ε. First, the vorticity dynamics in the upper layer is frozen in time:

$$
\partial_t \omega_1 = 0,
\tag{31}
$$

which we further simplify by initializing $\omega_1(x,y,0) = 0$. Together with $D_1 = 0$, this explains why it is asymptotically allowed to take $\mathbf{v}_1 = 0$ at leading order, as we discussed at the end of section §2.

Second, the balanced dynamics in the lower layer then becomes:

$$
\frac{\partial \mathbf{v}_2}{\partial t} = -q_2 \nabla^\perp \frac{\delta \mathcal{H}_0}{\delta \mathbf{v}_2} - \nabla \frac{\delta \mathcal{H}_0}{\delta \sigma_2}, \quad \text{and} \quad \frac{\partial \sigma_2}{\partial t} = -\nabla \cdot \frac{\delta \mathcal{H}_0}{\delta \mathbf{v}_2},
\tag{32}
$$

with $\mathcal{H}_0$ arising from (23) as the leading-order Hamiltonian on the constrained manifold (cf. (B5) with $\mathbf{v}_1 = 0$):

$$
\mathcal{H}_0 = \iint \left[\frac{1}{2} \sigma_2 |\mathbf{v}_2|^2 + (\sigma_1' + \sigma_2) z_2 \right.
$$
$$
\left. + \frac{1}{2} \theta_2 \kappa \Sigma_1^{\kappa-1} \left((\sigma_1' + \sigma_2)^2 - \sigma_2^2 \right) + \frac{1}{2} \theta_1 \kappa \Sigma_1^{\kappa-1} \sigma_1'^2 \right] dx\,dy.
\tag{33}
$$

Variation of (33) gives (cf. (D1) with $M_1'|_{\varepsilon=0} = 0$):

$$
\begin{aligned}
\delta \mathcal{H}_0 &= \iint \left[\sigma_2 \mathbf{v}_2 \cdot \delta \mathbf{v}_2 + \left(\frac{1}{2} |\mathbf{v}_2|^2 + M_2|_{\varepsilon=0} \right) \delta \sigma_2 + M_1'|_{\varepsilon=0} \delta \sigma_1' \right] dx\,dy, \\
&= \iint \left[\sigma_2 \mathbf{v}_2 \cdot \delta \mathbf{v}_2 + \left(\frac{1}{2} |\mathbf{v}_2|^2 + M_2|_{\varepsilon=0} \right) \delta \sigma_2 \right] dx\,dy,
\end{aligned}
\tag{34}
$$

using the constraint $M_1'|_{\varepsilon=0} = 0$, see equations (12) and (13). Alternatively, by including higher order terms in ε and using the (higher-order) constraint $M_1' = 0$ in the Hamiltonian, we can use the original Hamiltonian (23) on the constrained manifold $\mathbf{v}_1 = 0$ (by initializing $\omega_1(x, y, 0) = 0$) and $M_1' = 0$. The generalized Poisson bracket is then truncated to leading order on the (leading-order) constrained manifold, but the Hamiltonian $\mathcal{H}_{\mathbf{v}_1=0, M_1'=0}$ includes higher-order terms in ε. When we truncate this higher-order Hamiltonian one finds again $\mathcal{H}_0$, of course, as $\mathcal{H}_{\mathbf{v}_1=0, M_1'=0} \to_{\varepsilon \to 0} \mathcal{H}_0$ with $M_1'|_{\varepsilon=0} = 0$. This reduced Hamiltonian is chosen because it simply amounts to setting $\mathbf{v}_1 = 0$ and $z_0 = Z_0$ to get the rigid-lid approximation $M_1' = 0$ in the Hamiltonian, which provides a physical procedure for our approximation.

The dynamics on the constrained manifold is governed by the slow variables $\{\omega_1 = 0, \mathbf{v}_2, \sigma_2\}$, since the dynamics of the fast variables $\{D_1, \sigma_1'\}$ or $\{D_1, \phi_1\}$ associated with the gravity waves in the top layer is absent at leading order. Restricting or truncating the transformed bracket (26) to the constrained manifold and keeping all leading-order terms in ε, the following (dimensional and dimensionless) constrained dynamics emerges:

$$\frac{d\mathcal{F}_c}{dt} = \{\mathcal{F}_c, \mathcal{H}_c\}_c = \iint \left[q_2 \frac{\delta \mathcal{F}_c}{\delta \mathbf{v}_2}^{\perp} \cdot \frac{\delta \mathcal{H}_c}{\delta \mathbf{v}_2} - \frac{\delta \mathcal{F}_c}{\delta \sigma_2} \boldsymbol{\nabla} \cdot \frac{\delta \mathcal{H}_c}{\delta \mathbf{v}_2} + \frac{\delta \mathcal{H}_c}{\delta \sigma_2} \boldsymbol{\nabla} \cdot \frac{\delta \mathcal{F}_c}{\delta \mathbf{v}_2} \right] dx\,dy, \tag{35}$$

with the constrained Hamiltonian either $\mathcal{H}_c = \mathcal{H}_0$ (with $M_1'|_{\varepsilon=0} = 0$) or $\mathcal{H}_c = \mathcal{H}_{\mathbf{v}_1=0, M_1=0}$. We emphasize that $\mathcal{F}_c$ and $\mathcal{H}_c$ are functionals of the slow variables $\mathbf{v}_2$ and σ_2 only.

5.2 The Jacobi identity

The bracket (35) satisfies the Jacobi identity since it coincides with the bottom layer terms in the original bracket (21), which consists of two uncoupled parts, one for each layer, to which the Jacobi identity can be applied separately. In this sense, the preservation of the Jacobi identity for the leading-order reduced bracket (35) is straightforward to prove in the asymptotic analysis presented in this paper. However, proving the Jacobi identity for the leading-order reduced bracket resulting from a singular perturbation approach in the general case is more complicated and we refer to Bokhove (1996, 2002a) for a more extensive discussion of this topic.

5.3 Dimensional dynamics

Finally, the dynamics on the constrained manifold is given by (15) for $\mathcal{F} = \mathcal{F}_c$ and $\mathcal{H} = \mathcal{H}_c$ with (35) and the dimensional constrained Hamiltonian

$$\begin{aligned}
\mathcal{H}_c = \iint \Bigg[&\frac{1}{2} \sigma_2 |\mathbf{v}_2|^2 + g(\sigma_1 + \sigma_2) z_2 + \frac{c_p p_r \theta_2}{g(\kappa+1)} (\eta_2^{\kappa+1} - \eta_1^{\kappa+1}) \\
&+ \frac{c_p p_r \theta_1}{g(\kappa+1)} \eta_1^{\kappa+1} - \sigma_1 (c_p \theta_1 \eta_0^{\kappa} + g Z_0) \Bigg] dx\,dy,
\end{aligned} \tag{36}$$

with $\sigma_2 = (p_2 - p_1)/g$, $\sigma_1 = p_1/g$, and the constraint $M_1 = 0$ (i.e. $z_0 = Z_0$) relating $\eta_1 = p_1/p_r$ to $\eta_2 = p_2/p_r$, that is,

$$M_1 = c_p \theta_2 \eta_2^{\kappa} + c_p (\theta_1 - \theta_2) \eta_1^{\kappa} + g(z_2 - Z_0) = 0. \tag{37}$$

As argued earlier, instead of using the constrained Hamiltonian truncated to leading order in ε, we use the original Hamiltonian reduced to the constraint, or "rigid-lid" manifold, $M_1 = 0$ (and $\mathbf{v}_1 = 0$). Hence, we include higher-order terms in ε in the Hamiltonian. This does not hamper the leading-order accuracy since the constrained bracket (35) is leading order. The functional derivative of the potential and internal energy in (36) subject to constraint (37) is:

$$\begin{aligned}
\frac{\delta \mathcal{H}_{ci}}{\delta \sigma_2} \delta \sigma_2 &= \left(z_2 + \frac{c_p \theta_2}{g} \eta_2^{\kappa} \right) \delta p_2 + \left(\frac{c_p (\theta_1 - \theta_2)}{g} \eta_1^{\kappa} - Z_0 \right) \delta p_1 \\
&= \left(z_2 + \frac{c_p \theta_2}{g} \eta_2^{\kappa} \right) \delta p_2 + \left(\frac{c_p (\theta_1 - \theta_2)}{g} \eta_1^{\kappa} - Z_0 \right) \frac{\partial p_1}{\partial p_2} \delta p_2 \\
&= \left(z_2 + \frac{c_p \theta_2}{g} \eta_2^{\kappa} \right) \left(1 - \frac{\partial p_1}{\partial p_2} \right) \delta p_2 = M_2 \, \delta \sigma_2,
\end{aligned} \tag{38}$$

using the definition $g \sigma_2 = p_2 - p_1$ and with $\mathcal{H}_{ci}[\sigma_2] = \mathcal{H}_c[\mathbf{v}_2 = 0, \sigma_2]$ denoting the non-kinetic terms in the Hamiltonian. The equations of motion (3) for $\alpha = 2$ thus stay the same with Montgomery potential (3c), in which σ_1 is defined in terms of σ_2 and z_2 by $M_1 = 0$ via (3d).

Recapitulating, we note that we have been able to construct the Hamiltonian formulation of an isentropic 1.5-layer model. Importantly, we conclude *a posteriori* that it is consistent to set $\mathbf{v}_1 = 0$, since in the upper layer we found $\omega_1 = 0$ by initializing $\omega_1(x, y, 0) = 0$ and $D_1 = 0$ in the small ε limit.

6 Conclusions

In this paper, Part II, we have provided a full mathematical derivation of the isentropic $1\frac{1}{2}$-layer shallow water model utilised in Part I. Starting from an isentropic two-layer model, we show how a rigid-lid constraint alone (leading to the condition on the Montgomery potential in the top layer $M_1 = 0$) does not suffice to derive an entirely consistent $1\frac{1}{2}$-layer model, resulting instead in an apparent inconsistent configuration due to the non-preservation in time of the $M_1 = 0$ constraint.

To resolve this apparent inconsistency, we have shown how the $1\frac{1}{2}$-layer model emerges from the two-layer one, once the latter is properly scaled to allow for the asymptotic analysis. In the limit $\varepsilon = U_1/U_2 \to 0$, two constraints emerge, i.e. $M_1 = 0$ and $\mathbf{v}_1 = 0$, and the system reduces to a single set of equations for the (slow) variables in the bottom layer.

We have further demonstrated that the scaling used in the asymptotic analysis can be justified on the basis of real observations; these arise in both the modelling of a two-layer stratosphere and that of a two-layer troposphere in the presence of a Low-Level Jet. The latter is the most useful in view of using the idealised model described in Part I for satellite data assimilation research. Finally, a Hamiltonian derivation of the model has been undertaken in section §5, where a slaved Hamiltonian approach has been used – generalized here for the infinite-dimensional case – thus removing an apparent inconsistency in the model derivation as well as underpinning the conservative nature of the system.

Appendices

A Dimensionless Montgomery potentials in the scaled equations

In this appendix we show how to obtain the expressions of the dimensionless Montgomery potentials M_1' and M_2' in (11). First, we notice that the non-dimensionalization of the momentum equations in (3) using (8) leads to the dimensionless terms:

$$\frac{1}{\varepsilon^3}\nabla M_1^*, \quad \text{and} \quad \frac{1}{\text{Fr}_2^2}\nabla M_2^* \tag{A1}$$

with M_1^* and M_2^* being:

$$M_1^* = \theta_2^*\eta_2^\kappa + (\theta_1^* - \theta_2^*)\eta_1^\kappa - \theta_1^*\eta_0^\kappa - Z_0^* + \varepsilon^2 z_2^*, \tag{A2}$$

$$M_2^* = \frac{1}{\delta_a}\theta_2^*\eta_2^\kappa + \text{Fr}_2^2 z_2^*, \tag{A3}$$

after adding the constant K to M_1. Therefore, we define the (constant) mean potentials $\bar{M}_1$ and $\bar{M}_2$:

$$\bar{M}_1 = \theta_1^*\Sigma_1^\kappa - \theta_1^*\eta_0^\kappa - Z_0^*, \tag{A4}$$

$$\bar{M}_2 = \frac{1}{\delta_a}\theta_2^*\Sigma_1^\kappa, \tag{A5}$$

which can be subsequently subtracted from M_1^* and M_2^* in (A1), as it is always possible to vary a potential by a constant without loss of generality. Finally, by bringing a factor $1/\varepsilon^2$ inside ∇M_1^* and a factor $1/\text{Fr}_2^2$ inside ∇M_2^* in (A1), we can define the quantities:

$$M_1' = (M_1^* - \bar{M}_1)/\varepsilon^2, \tag{A6}$$

$$M_2' = (M_2^* - \bar{M}_2)/\text{Fr}_2^2, \tag{A7}$$

which together with (6) lead to the expressions in (11).

B   Scaled Hamiltonian of a two-layer shallow water model

The scaled Hamiltonian displayed in eq. (23) can be obtained by multiplying the dimensional two-layer Hamiltonian in (17) by a factor $g/(p_r U_2^2 \varepsilon^2 L^2)$ and by applying the scaling in (8). This leads to the expression:

$$
\mathcal{H} = \iint \left[\frac{1}{2}(\Sigma_1 + \varepsilon^2 \sigma_1')|\mathbf{v}_1|^2 + \frac{1}{\varepsilon^2}\Sigma_1 z_2 + \sigma_1' z_2 + \frac{1}{2}\sigma_2|\mathbf{v}_2|^2 + \sigma_2 z_2 + \right.
$$
$$
\left. + \frac{1}{\varepsilon^4(\kappa+1)}\theta_2\left(\eta_2^{\kappa+1} - \eta_1^{\kappa+1}\right) + \frac{1}{\varepsilon^4(\kappa+1)}\theta_1\eta_1^{\kappa+1} - \frac{1}{\varepsilon^4}\left(\theta_1\eta_0^{\kappa} + Z_0\right)(\Sigma_1 + \varepsilon^2 \sigma_1') \right] \mathrm{dxdy},
$$
(B1)

which can be conveniently modified by adding the Casimirs invariants:

$$
C_1 = \lambda_1 \iint (\Sigma_1 + \varepsilon^2 \sigma_1')\mathrm{dxdy},
$$
(B2)

$$
C_2 = \lambda_2 \iint (\varepsilon^2 \sigma_2)\mathrm{dxdy},
$$
(B3)

with:

$$
\lambda_1 = \frac{1}{\varepsilon^4}\left(\theta_1\eta_0^{\kappa} + Z_0 - \theta_1\Sigma_1^{\kappa}\right) \quad \text{and} \quad \lambda_2 = -\frac{1}{\varepsilon^4}\theta_2\Sigma_1^{\kappa},
$$
(B4)

and by neglecting the constant term $\frac{1}{\varepsilon^2}\Sigma_1 z_2$.

In doing so, the obtained scaled Hamiltonian (23) is non-singular at order $O(1)$ for $\varepsilon \to 0$, that is:

$$
\mathcal{H} = \iint \left[\frac{1}{2}\Sigma_1|\mathbf{v}_1|^2 + \frac{1}{2}\sigma_2|\mathbf{v}_2|^2 + (\sigma_1' + \sigma_2)z_2 + \frac{1}{2}\kappa\theta_1\Sigma_1^{\kappa-1}\sigma_1'^2 + \frac{1}{2}\kappa\theta_2\Sigma_1^{\kappa-1}(\sigma_2^2 + 2\sigma_1'\sigma_2) \right] \mathrm{dxdy}.
$$
(B5)

The expression above is obtained by computing the Taylor expansion of (23) around $(\sigma_1' = 0, \sigma_2 = 0)$ and by retaining only the terms at leading order in ε, with $\varepsilon \to 0$.

C   Change of variables in the functional derivatives

In this appendix we show how to compute the functional derivatives with respect to the initial variables $(\sigma_1', \sigma_2, \mathbf{v}_1, \mathbf{v}_2)$ in terms of those derived in the asymptotic analysis $(D_1, \omega_1, \phi_1, \sigma_2, \mathbf{v}_2)$. We start from the definition of the differential $\delta\mathcal{F}$ written in terms of both set of variables:

$$
\delta\mathcal{F} = \iint \left[\frac{\delta\mathcal{F}}{\delta\sigma_1'}\delta\sigma_1' + \frac{\delta\mathcal{F}}{\delta\sigma_2}\delta\sigma_2 + \frac{\delta\mathcal{F}}{\delta\mathbf{v}_1}\delta\mathbf{v}_1 + \frac{\delta\mathcal{F}}{\delta\mathbf{v}_2}\delta\mathbf{v}_2 \right] \mathrm{dxdy};
$$
(C1)

$$
\delta\mathcal{F} = \iint \left[\frac{\delta\mathcal{F}}{\delta D_1}\delta D_1 + \frac{\delta\mathcal{F}}{\delta\omega_1}\delta\omega_1 + \frac{\delta\mathcal{F}}{\delta\phi_1}\delta\phi_1 + \frac{\delta\mathcal{F}}{\delta\sigma_2}\delta\sigma_2 + \frac{\delta\mathcal{F}}{\delta\mathbf{v}_2}\delta\mathbf{v}_2 \right] \mathrm{dxdy}.
$$
(C2)

By exploiting the relationships between one set of variables and the other, we can equate the terms in (C1) and (C2) that depend on the same differential. For example, since both D_1 and ω_1 are functions of $\mathbf{v}_1$, we can write:

$$
\iint \left[\frac{\delta\mathcal{F}}{\delta\mathbf{v}_1}\delta\mathbf{v}_1 \right] \mathrm{dxdy} = \iint \left[\frac{\delta\mathcal{F}}{\delta D_1}\delta D_1 + \frac{\delta\mathcal{F}}{\delta\omega_1}\delta\omega_1 \right] \mathrm{dxdy}
$$
$$
= \iint \left[\nabla \cdot \left(\Sigma_1 \frac{\delta\mathcal{F}}{\delta D_1}\delta\mathbf{v}_1 \right) - \Sigma_1 \delta\mathbf{v}_1 \nabla \frac{\delta\mathcal{F}}{\delta D_1} + \right.
$$
$$
\left. + \nabla^{\perp} \cdot \left(\frac{\delta\mathcal{F}}{\delta\omega_1}\delta\mathbf{v_1} \right) - \delta\mathbf{v}_1 \nabla^{\perp}\frac{\delta\mathcal{F}}{\delta\omega_1} \right] \mathrm{dxdy}
$$
$$
= \iint \left[\left(-\Sigma_1\nabla\frac{\delta\mathcal{F}}{\delta D_1} - \nabla^{\perp}\frac{\delta\mathcal{F}}{\delta\omega_1} \right)\delta\mathbf{v}_1 \right] \mathrm{dxdy},
$$
(C3)

in which the divergence terms are zero due to the boundary conditions. In the expression above the differentials δD_1 and $\delta\omega_1$ have been computed as:

$$
\delta D_1 = \delta(\nabla \cdot (\Sigma_1 \mathbf{v}_1)) = \nabla \cdot (\Sigma_1 \delta\mathbf{v}_1),
$$
(C4)
$$
\delta\omega_1 = \delta(\nabla^{\perp} \cdot \mathbf{v}_1) = \nabla^{\perp} \cdot \delta\mathbf{v}_1.
$$
(C5)

The functional derivatives with respect to the other variables can be obtained accordingly.

D Scaled variational Hamiltonian in the limit $\varepsilon \to 0$

Taking the variation of (B5) one obtains:

$$
\begin{aligned}
\delta \mathcal{H} = \iint \Bigg[& \Sigma_1 \mathbf{v}_1 \cdot \delta \mathbf{v}_1 + \sigma_2 \mathbf{v}_2 \cdot \delta \mathbf{v}_2 + \frac{1}{2}|\mathbf{v}_2|^2 \delta \sigma_2 + (\delta \sigma_1' + \delta \sigma_2) z_2 + \\
& + \kappa \theta_1 \Sigma_1^{\kappa-1} \sigma_1' \delta \sigma_1' + \kappa \theta_2 \Sigma_1^{\kappa-1} \left(\sigma_2 \delta \sigma_2 + \sigma_1' \delta \sigma_2 + \sigma_2 \delta \sigma_1' \right) \Bigg] \mathrm{d}x\mathrm{d}y \\
= \iint \Bigg[& \Sigma_1 \mathbf{v}_1 \cdot \delta \mathbf{v}_1 + \sigma_2 \mathbf{v}_2 \cdot \delta \mathbf{v}_2 + M_1'|_{\varepsilon=0} \delta \sigma_1' + \left(\frac{1}{2}|\mathbf{v}_2|^2 + M_2'|_{\varepsilon=0} \right) \delta \sigma_2 \Bigg] \mathrm{d}x\mathrm{d}y
\end{aligned}
\tag{D1}
$$

in which eqs. (13) have been used. The first term in the integral above (a velocity) can be rewritten in terms of a potential χ and a streamfunction Ψ, i.e. $\Sigma_1 \mathbf{v}_1 = \Sigma_1 \nabla \chi + \nabla^\perp \Psi$, and subsequently manipulated as follows (using common vector calculus identities):

$$
\begin{aligned}
\iint \left[\Sigma_1 \mathbf{v}_1 \cdot \delta \mathbf{v}_1 \right] \mathrm{d}x\mathrm{d}y &= \iint \left[\left(\Sigma_1 \nabla \chi + \nabla^\perp \Psi \right) \cdot \delta \mathbf{v}_1 \right] \mathrm{d}x\mathrm{d}y \\
&= \iint \left[\Sigma_1 \nabla \chi \cdot \delta \mathbf{v}_1 \right] \mathrm{d}x\mathrm{d}y + \iint \left[\nabla^\perp \Psi \cdot \delta \mathbf{v}_1 \right] \mathrm{d}x\mathrm{d}y \\
&= \iint \left[\nabla \cdot (\Sigma_1 \chi \delta \mathbf{v}_1) - \chi \nabla \cdot (\Sigma_1 \delta \mathbf{v}_1) \right] \mathrm{d}x\mathrm{d}y \\
&\quad + \iint \left[\nabla^\perp \cdot (\Psi \delta \mathbf{v}_1) - \Psi \nabla^\perp \cdot \delta \mathbf{v}_1 \right] \mathrm{d}x\mathrm{d}y \\
&= \iint \left[\nabla \cdot (\Sigma_1 \chi \delta \mathbf{v}_1) - \chi \delta D_1 \right] \mathrm{d}x\mathrm{d}y + \iint \left[\nabla^\perp \cdot (\Psi \delta \mathbf{v}_1) - \Psi \delta \omega_1 \right] \mathrm{d}x\mathrm{d}y \\
&= \iint \left[-\chi \delta D_1 - \Psi \delta \omega_1 \right] \mathrm{d}x\mathrm{d}y
\end{aligned}
\tag{D2}
$$

in which the divergence terms are zero due to the boundary conditions and the definitions of the differentials δD_1 and $\delta \omega_1$ in (C4) have been used.

References

Birner, T., 2006: Fine-scale structure of the extratropical tropopause region. *Journal of Geophysical Research: Atmospheres*, **111 (D4)**.

Bokhove, O., 1996: On balanced models in geophysical fluid dynamics: slowest invariant manifolds, slaving principles, and hamiltonian structure. Ph.D. thesis, University of Toronto.

Bokhove, O., 2002a: Balanced models in geophysical fluid dynamics: Hamiltonian formulation, constraints and formal stability. *Large-Scale Atmosphere-Ocean Dynamics 2, Geometric Methods and Models*, J. Norbury, and I. Roulstone, Eds., Cambridge University Press.

Bokhove, O., 2002b: Eulerian variational principles for stratified hydrostatic equations. *Journal of the atmospheric sciences*, **59 (9)**, 1619–1628.

Bokhove, O., 2007: Constrained 1.5-layer hamiltonian toy models for stratospheric dynamics, available at http://www1.maths.leeds.ac.uk/~obokhove/bokhove07rev.pdf.

Bokhove, O., and M. Oliver, 2009: Hamiltonian n–layer model for atmospheric dynamics. *Geophys. Astrophys. Fluid Dyn*, **103 (6)**, 423–442.

Cantarello, L., O. Bokhove, and S. Tobias, 2021: An idealized $1\frac{1}{2}$-layer isentropic model with convection and precipitation for satellite data assimilation research. Part I: model dynamics, preprint available at https://eartharxiv.org/repository/view/2006/.

Dirac, P., 1964: Lectures on quantum mechanics, yeshiva university. *New York*, 40–66.

Dirac, P. A. M., 1958: Generalized hamiltonian dynamics. *Proceedings of the Royal Society of London. Series A. Mathematical and Physical Sciences*, **246 (1246)**, 326–332.

Djurić, D., and M. S. Damiani Jr, 1980: On the formation of the low-level jet over texas. *Monthly Weather Review*, **108 (11)**, 1854–1865.

Kent, T., O. Bokhove, and S. Tobias, 2017: Dynamics of an idealized fluid model for investigating convective-scale data assimilation. *Tellus A: Dynamic Meteorology and Oceanography*, **69 (1)**, 1369 332.

Ladwig, D. S., 1980: Cyclogenesis and the low-level jet over the southern great plains. Tech. rep., AIR FORCE INST OF TECH WRIGHT-PATTERSON AFB OH.

Rife, D. L., J. O. Pinto, A. J. Monaghan, C. A. Davis, and J. R. Hannan, 2010: Global distribution and characteristics of diurnally varying low-level jets. *Journal of Climate*, **23 (19)**, 5041–5064.

Ripa, P., 1993: Conservation laws for primitive equations models with inhomogeneous layers. *Geophysical & Astrophysical Fluid Dynamics*, **70 (1-4)**, 85–111.

Salman, H., L. Kuznetsov, C. Jones, and K. Ide, 2006: A method for assimilating lagrangian data into a shallow-water-equation ocean model. *Monthly Weather Review*, **134 (4)**, 1081–1101.

Salmon, R., 1983: Practical use of hamilton's principle. *Journal of Fluid Mechanics*, **132**, 431–444.

Salmon, R., 1985: New equations for nearly geostrophic flow. *Journal of Fluid Mechanics*, **153**, 461–477.

Salmon, R., 1988: Hamiltonian fluid mechanics. *Annual review of fluid mechanics*, **20 (1)**, 225–256.

Shepherd, T., 1990: Symmetries, conservation laws, and hamiltonian structure in geophysical fluid dynamics. *Adv. Geophys*, **32 (287-338)**, 2.

Stewart, L. M., S. L. Dance, and N. K. Nichols, 2013: Data assimilation with correlated observation errors: experiments with a 1-d shallow water model. *Tellus A: Dynamic Meteorology and Oceanography*, **65 (1)**, 19 546.

Vallis, G., 2017: *Atmospheric and oceanic fluid dynamics*. Cambridge University Press.

Van Kampen, N. G., 1985: Elimination of fast variables. *Physics Reports*, **124 (2)**, 69–160.

Vanneste, J., and O. Bokhove, 2002: Dirac-bracket approach to nearly geostrophic hamiltonian balanced models. *Physica D: Nonlinear Phenomena*, **164 (3-4)**, 152–167.

Würsch, M., and G. C. Craig, 2014: A simple dynamical model of cumulus convection for data assimilation research. *Meteorologische Zeitschrift*, **23 (5)**, 483–490.

Žagar, N., N. Gustafsson, and E. Källén, 2004: Dynamical response of equatorial waves in four-dimensional variational data assimilation. *Tellus A: Dynamic Meteorology and Oceanography*, **56 (1)**, 29–46.

Zeitlin, V., 2007: *Nonlinear dynamics of rotating shallow water: Methods and advances*. Elsevier.
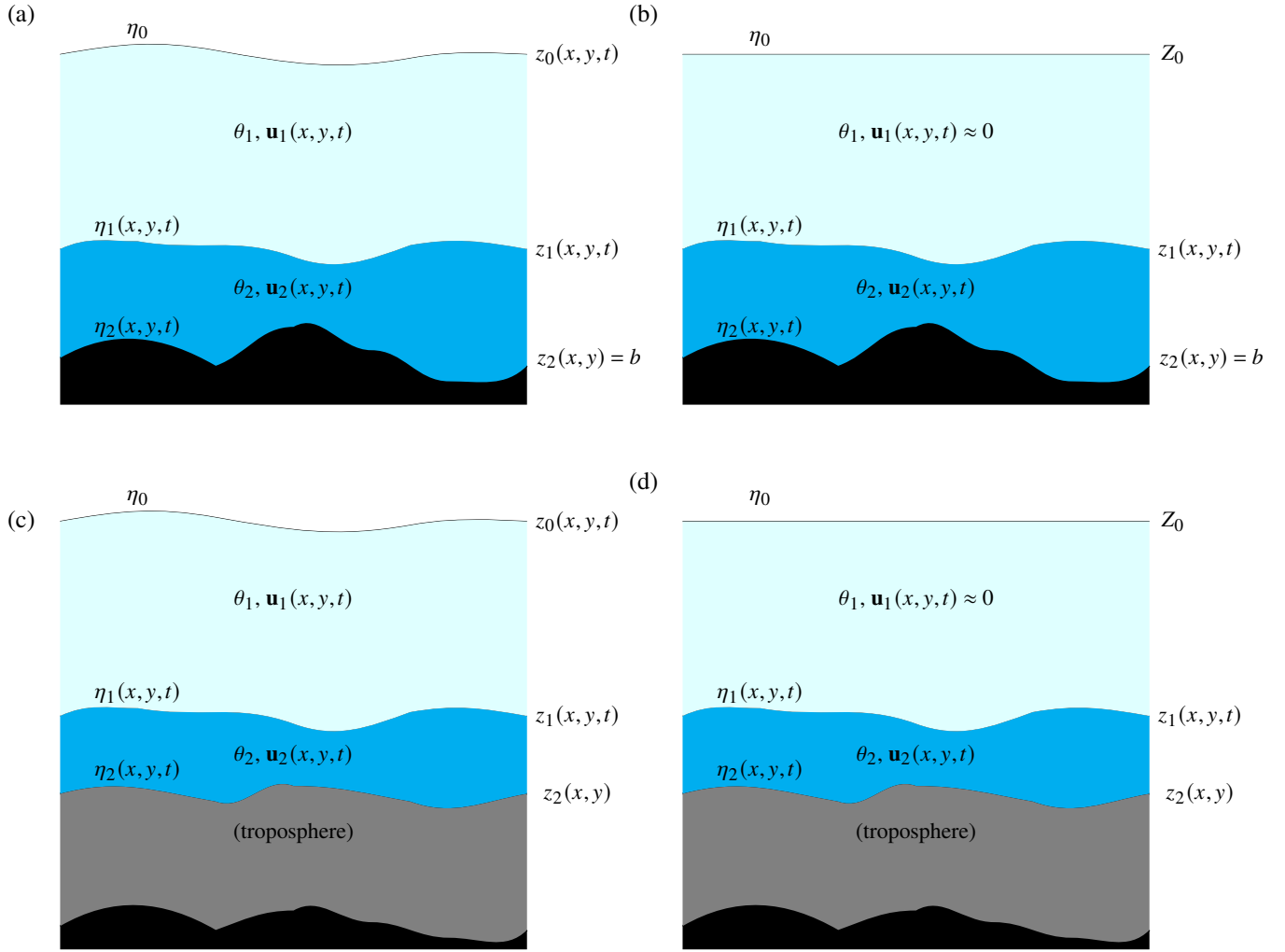
Figure 1: Schematic representation of the isentropic shallow water model with associated variables in the troposphere (top panels: a,b) and in the stratosphere (bottom panels: c,d) for a two-layer (left panels: a,c) and a $1\frac{1}{2}$-layer approximation (right panels: b,d). In the $1\frac{1}{2}$-layer model the top layer is at rest (i.e. $\mathbf{u}_1(x,y,t) \approx 0$) and is capped by a rigid lid (i.e. $z(x,y,t) = Z_0$).

	two-layer stratosphere	two-layer troposphere (Low-Level-Jet)			
	Fig. 2	Fig. 3(a)	Fig. 3(b)	Fig. 3(c)	Average
H_2 [km]	6	2.02	2.08	1.65	1.92
H_1 [km]	18	3.98	4.02	4.6	4.2
p_0^{obs} [mbar]	6.2	489.6	483.8	475.4	482.9
p_1^{obs} [mbar]	97	805.0	801.3	843.7	816.7
p_2^{obs} [mbar]	242	1026	1028	1027	1027
θ_1^{obs} [K]	672	311.0	311.0	311.0	311.0
θ_2^{obs} [K]	381	291.8	291.8	291.8	291.8
U_1^{obs} [m/s]	2	3.6	6.6	7.0	5.7
U_2^{obs} [m/s]	14	13.5	12.7	11.0	12.4
Fr_1^{obs}	0.0048	0.018	0.033	0.033	0.028
Fr_2^{obs}	0.0577	0.096	0.089	0.086	0.090
δ_a	0.33	0.51	0.52	0.36	0.46
ε	0.14	0.27	0.52	0.64	0.46
$\text{Fr}_1 \approx \varepsilon^2$	0.02	0.073	0.27	0.41	0.21
$\text{Fr}_2 \approx \frac{\varepsilon}{\sqrt{\delta_a}}$	0.24	0.38	0.72	1.07	0.68
p_1 [mbar]	97	804.6	800.2	843.2	—
θ_1 [K]	629	312.2	311.5	311.9	—

Table 1: Summary of the values of various physical quantities obtained from the radiosonde data displayed in Figs. 2-3 and resulting values of non-dimensional scaling parameters δ_a and ε. The values of Fr_1 and Fr_2 –scaling hypotheses made earlier in section 3– are also reported. The values of p_1 and θ_1 in the bottom rows are computed via (5) using the observed quantities p_0^{obs}, p_2^{obs}, H_1^{obs}, H_2^{obs} and θ_2^{obs}. The rightmost column reports the average values obtained from the data seen in Fig. 3.
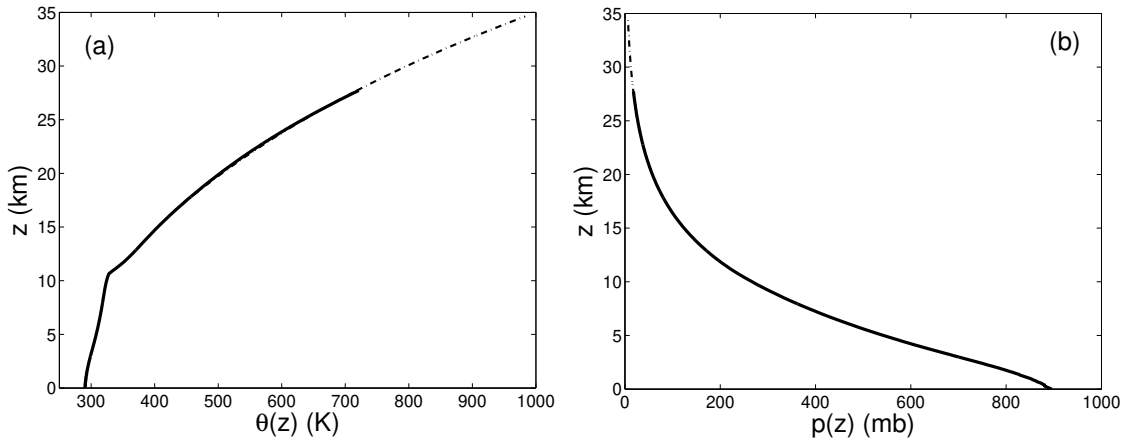

Figure 2: Profiles, zonally averaged, (solid lines) of (a) observed potential temperature $\theta(z)$ and (b) pressure $p(z)$ versus height z at circa 57.25° N, and extrapolated profiles (dash-dotted lines) from $Z_1 = 16.63$ km to $Z_0 = 34.63$ km based on the approximately constant scale heights of the observed θ and p, respectively, in the stratosphere. The tropopause lies at approximately $Z_2 = 10.63$ km. Data courtesy Dr. Thomas Birner (cf. Birner (2006)). The relevant physical parameters associated with these vertical profiles are reported in Table 1.
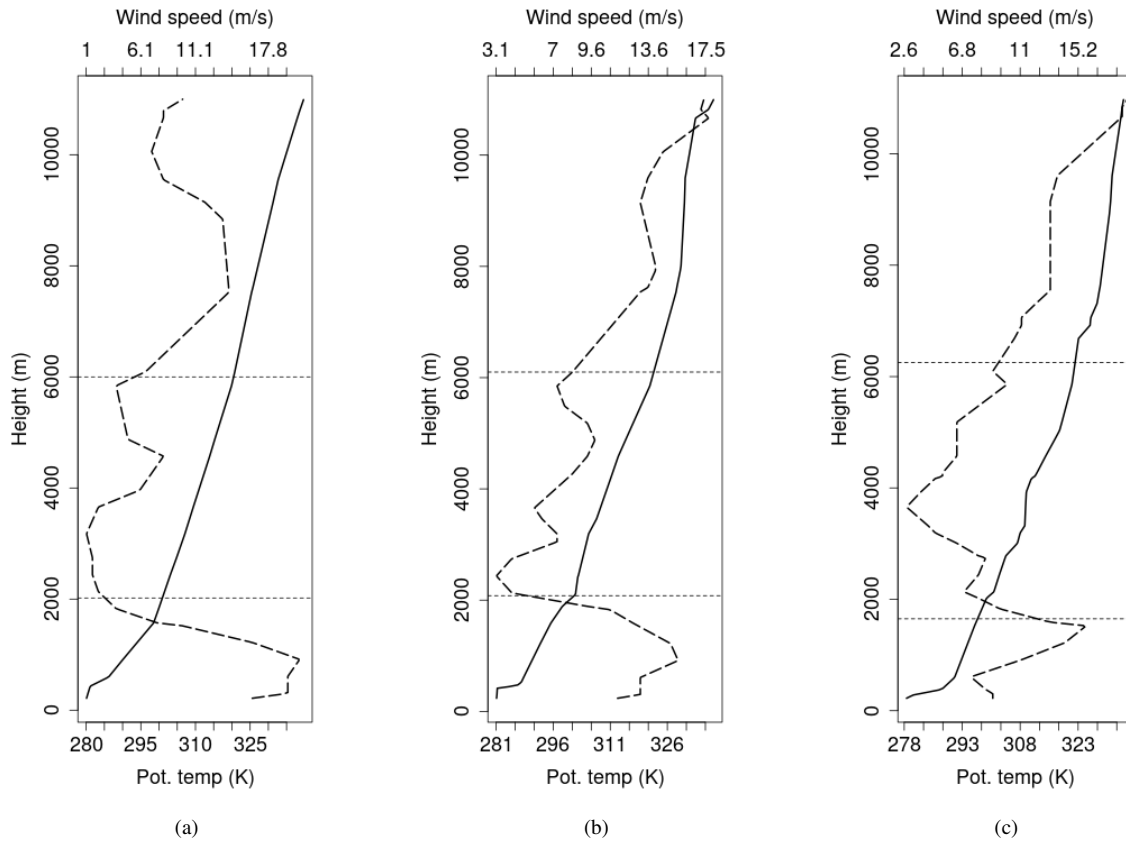
Figure 3: Vertical profile of potential temperature (solid line) and wind speed (dashed line) taken from radiosonde data on (a) 10/12/1977 at 00Z, (b) 10/12/1977 at 12Z and (c) 11/12/1977 at 00Z in Brownsville, Texas (US). The horizontal dotted lines indicate the depth of the two layers deduced from potential temperature data. The relevant physical parameters associated with each vertical profile are reported in Table 1. Source: http://weather.uwyo.edu/upperair/sounding.html